ELSEVIER

Journal of Nuclear Materials 301 (2002) 122–128

journal of nuclear materials

www.elsevier.com/locate/jnucmat

Competition between disorder creation and annealing in fluoroapatite nuclear waste forms

J. Chaumont [a,*], S. Soulet [a,b], J.C. Krupa [c], J. Carpena [b]

[a] *Centre de Spectrométrie Nucléaire et de Spectrométrie de Masse, CNRS-IN2P3, Bat 104-108, 91405 Orsay Campus, France*

[b] *CEA-Cadarache, DESD/SEP/LEMC, 13108 Saint-Paul-lez-Durance, France*

[c] *Institut de Physique Nucléaire, CNRS-IN2P3, 91406 Orsay cedex, France*

Received 27 July 2001; accepted 29 November 2001

Abstract

He-ion irradiation simulating α-particle emission, induces crystal defect recovery in fluoroapatite $Ca_{10}(PO_4)_6F_2$ pre-damaged by Pb-ions. In fluoroapatite loaded with α-emitter actinides, a similar effect is expected. Therefore, the amorphization level in fluoroapatite has been modeled versus disposal time, α-decay fluence and temperature. When loaded with ^{239}Pu and ^{244}Cm, the structural disorder reaches a plateau, which level depends only slightly on α-energies. This level corresponds to an amorphous fraction of approximately 20% of disorder and is independent of the dose rate. The time delay in reaching the equilibrium regime in the disorder production is inversely proportional to the dose rate whereas the dose or the actinide content is not a critical parameter for the magnitude of the equilibrium level.

PACS: 61.72.Cc; 61.80.Az

1. Introduction

Materials that are chemically and thermally stable over geologic periods are needed for the immobilization of high level radioactive α-emitters in a deep geological repository. The material behavior under radiation is one of the main factors to be considered. Indeed, radiation can affect considerably the chemical durability when a crystalline to amorphous transformation occurs. The associated volume changes can lead to micro-fractures or even a large fractionating of the waste form. Therefore, the choice among different potential host matrices should be based on two factors: amorphization susceptibility and kinetics of the aqueous dissolution, taking into account that the total fluence during disposal time may be up to 20 times larger than that required for amorphization. Hence, it is essential to search for materials in which the amorphizability is balanced by a high tendency to recrystallize.

Actinide-containing minerals studies suggest that apatites are potential nuclear waste disposal materials [1–5]. One of the most convincing proofs of the apatite radiation resistance was provided by apatitic minerals from Ouzzal mole in Hoggar (Algeria), which were shown to have incorporated actinides such as U and Th [6,7]. Some of these apatites have sustained high doses of radioactivity ranging from 1×10^{19} to 3×10^{19} α events g^{-1} though they are readily amorphized by ion-beams that simulate α-recoils. Then, only their ability to anneal radiation damages explains their crystallinity.

Regarding the very high radiotoxicity and the long lifetimes of α-emitters, the safest storage condition will be offered by the crystalline state provided that the total amorphization of the solid waste form is prevented during the disposal time. However, this condition is not sufficiently safe because a large increase of the leach rate

* Corresponding author. Tel.: +33-1 69 15 52 88; fax: +33-1 69 15 52 68.

E-mail address: chaumont@csnsm.in2p3.fr (J. Chaumont).

0022-3115/02/$ - see front matter
PII: S0022-3115(01)00758-9

Fig. 1. Preferential dissolution by an acidic solution of neutron-induced fission tracks in a natural fluoroapatite.

may also be caused by a percolation phenomenon [8] between highly disordered zones. As a matter of fact, if for low defect concentrations, only the damaged regions at the surface can be easily dissolved, for high disordered zone concentrations, continuous paths may be created providing for preferential dissolution deep into the matrix. Such a dissolution process can be evidenced when fission tracks are etched by acidic solutions as observed for a natural fluoroapatite (Fig. 1). Open channels inside the ceramics induce a large increase of the leached surface area, which was not yet considered. But, as the geometrical shape of the disordered volume created by an α-decay event is not well defined, it is difficult to evaluate the defect concentration threshold leading to percolation. For this reason, the disorder should always remain below the percolation threshold. That implies that the concentration of disordered volumes created by α-recoil nuclei remains low enough to consider these zones as isolated.

To be able to estimate the disorder level in a crystalline waste form at any disposal time, calculation requires measurements of the creation and annealing rates of isolated disordered zones at different temperatures. Based on previous experiments on disorder creation [10–12] and annealing kinetics [9] in fluoroapatite, we present a model of the disorder level evolution as a function of disposal time.

2. Disorder creation and annealing kinetics in fluoroapatite

2.1. Disorder creation in fluoroapatite

Direct impact model for amorphization was evidenced in fluoroapatite ($Ca_{10}(PO_4)_6F_2$) through transmission electronic microscopy experiments [10,13]. In the direct impact model, the average amorphized volume produced by every α-recoil at a temperature T, $V_0(T)$, takes already into account the thermally activated intracascade disorder annealing effect. $V_0(T)$ is decreasing with temperature and at temperatures higher than a critical temperature, T_c, which is characteristic of the material, amorphization will never occur ($V_0(T) = 0$).

Let be $dy_{creation}$, the increase of the disorder fraction created by a α-decay dose dD. The defect creation kinetics can be written as follows:

$$dy_{creation} = V_0(T)[1 - y]\,dD. \tag{1}$$

Then, when post-cascade disorder annealing is negligible, the disorder fraction, y, is given by [14,15]

$$y = 1 - \exp(-V_0(T)D). \tag{2}$$

The elementary damaged volume $V_0(T)$ can be evaluated from the initial slope of the amorphization curve and D is the cumulative α-decay dose. The product $V_0(T)D$ determines the disorder level and consequently the amorphization dose is inversely proportional to $V_0(T)$. When the direct impact model applies, the thermal evolution of $V_0(T)$ can be determined from the plots of the amorphization dose versus temperature, already reported for a large number of potential nuclear waste materials [11,16–22]. In the present study, $V_0(T)$ is determined from the magnitude of the disordered volume produced by a Pb-ion at temperature T.

2.2. Disorder α-annealing in fluoroapatite

Previous studies on Durango fluoroapatite single crystals, have shown that the isolated α-recoil disordered volumes simulated by 220 keV-Pb^{2+} ions are readily annealed at room temperature by the 1.6 MeV-helium beam used for RBS-C measurements [9]. In order to understand this epitaxial α-annealing phenomenon, other experiments were performed with different He-ion energies ranging from 0.3 to 3.2 MeV. These studies have shown that, in the energy range investigated, the amorphous fraction, y, decreases according to a mono-exponential law as a function of He-ion fluence, ϕ, following the equation

$$y = y_0 + y_1 \exp(-f\phi), \tag{3}$$

where y_0, is the initial disorder in sample, y_1 the disorder contribution due to Pb-ion irradiation and f, is the α-annealing cross-section depending on the chemical nature of the crystalline compounds. This equation assumes that only the disorder created by Pb-ion irradiation is recovered by He-ion annealing and not the initial disorder due to impurities, dislocations, surface damages and other damages that remain unaffected by α-annealing. As a matter of fact the χ_{min} determined on fluoroapatite was never improved by α-irradiation.

Since the He-ion intensity distribution and the real spot size used in RBS experiments are difficult to determine, the f-value in Eq. (3) is not very accurately evaluated. Nevertheless, when different calculated cross-sections are reported as a function of the α-particle energy, their trends follow the evolution of the electronic energy density deposited in the solid [9]. Consequently, two main characteristics of the α-annealing effect can be given:

(i) The annealing rate of isolated amorphous volumes is proportional to the electronic energy deposited by the α-particles in the solid. Then, the α-annealing cross-section, f, is proportional to the electronic stopping power, $\mathrm{d}E/\mathrm{d}x$ with a proportionality coefficient, $c(T)$, that is temperature dependent and corresponds to the volume recovery per eV. This coefficient depends on the matrix itself. The derivative of Eq. (3) becomes

$$\mathrm{d}y = -(yc(T)\,\mathrm{d}E/\mathrm{d}x)\,\mathrm{d}\phi. \tag{4}$$

(ii) Despite a defect recovery process that only operates at the crystalline to amorphous interface, the disorder annealing rate, $\mathrm{d}y$, has been measured to be proportional to the amorphous fraction y [9]. This proportionality means that only the energy deposited by inelastic interactions in the disordered volumes is efficient for the disorder annealing. It should be noted that Eq. (4) implies the existence of a large remaining crystalline fraction in the material and therefore $y = 1$ is totally excluded.

Additional α-annealing studies have been performed on a 80 nm thick amorphous layer created by 220 keV-Pb ions in a $Ca_{10}(PO_4)_6F_2$ single crystal cut perpendicularly to the c-axis [23]. 1.6 MeV-He ions have been used to produce α-annealing and to measure by RBS-C the evolution of the amorphous layer thickness. This thickness decreases linearly with the He-ion beam fluence while the Ca rear edge in RBS spectra moves without deformation towards the surface indicating that an epitaxial recrystallization occurs in the material. In contrast to electron annealing behavior [24] an important crystalline nucleation process in the amorphous phase can be excluded.

The disorder recovery rate at the interface between the amorphous layer and the underlying crystalline phase is about 2 atoms per He-ion whatever the layer thickness may be [23]. Now, if we consider isolated amorphous zones with a total volume corresponding to a 25 nm-thick fully amorphous layer, this recovery rate was estimated to reach about 60 atoms per 1.6 MeV-He ion [9]. This difference shows that the recovery at the interface of a fully amorphous layer is similar to the recovery in small isolated amorphous zones with a total amorphous volume corresponding to a 0.8 nm-thick layer only. This effect can be explained if the recovery process is generated by an undetermined active entity (a broken bond?) diffusing in the amorphous phase with a limited diffusion range. If a random diffusion process is assumed, an average range of 3 nm can be estimated in amorphous fluoroapatite. Therefore, when the amorphous fraction increases, the diffusion range can become smaller than the size of some amorphous domains and the efficiency of the recovery process will decrease accordingly. Consequently, for large amorphous fractions, Eq. (4) cannot be used.

The amorphous fraction corresponding to a decrease of α-annealing rate is difficult to calculate accurately because the geometry of α-recoil amorphous tracks is not well known. However, our RBS-experiments show that the amorphization rate, $\mathrm{d}y$, remains proportional to y when $y \leqslant 0.5$ to 0.6 [9].

2.2.1. Kinetics under disposal conditions

For the actual disposal conditions, RBS results have to be extended to a homogeneously doped waste form. In this case, two points have to be considered:

(i) the α-particle energy E. The α-particle energy distribution ranges from 0 to $E_{\max}$ at any given position in the solid. For fluoroapatite, the factor $c(T)$, standing for the volume recovery per eV at temperature T (see Eq. (4)) is independent of the α-particle energy and an average value $(\mathrm{d}E/\mathrm{d}x)_{\mathrm{av}}$ can be used for the energy density deposited along the α-particle range, R, in the waste form.

(ii) the α-flux ϕ in the waste form. In the actinide host phase, the α-flux evolution, $\mathrm{d}\phi$, is directly proportional to the dose rate $\mathrm{d}D$: ($\mathrm{d}\phi = k\,\mathrm{d}D$) whereas the dose rate depends on actinide concentrations and radioactive half-life of the considered nuclides. To determine the constant k, let us consider an elementary volume, $\mathrm{d}V$, located at a distance x from a plane. The number of α-particles with a range R, emitted from this elementary volume is $\mathrm{d}N = \mathrm{d}V\,\mathrm{d}D$. Their probability to cross the given plane can be written as $P = (R - x)/2R$ where P varies linearly from 0.5 at $x = 0$ to 0 at $x = R$ with an average value of 0.25. Therefore, the α-fluence through the given plane is equal to the number of α-particles emitted by a form layer of $R/4$ in thickness when only one side of the plane (i.e. at the surface of the form) is considered, or $R/2$ if both sides are taken into account. Thus, in the bulk, $k = R/2$, and the α-flux increment $\mathrm{d}\phi$ is equal to

$$\mathrm{d}\phi = (R/2)\,\mathrm{d}D.$$

Consequently, the disordered fraction evolution, $\mathrm{d}y$, under He-ion irradiation (Eq. (4)) in a homogeneously doped waste form can be written as

$$\mathrm{d}y = -c(T)y(\mathrm{d}E/\mathrm{d}x)_{\mathrm{av}}(R/2)\,\mathrm{d}D. \tag{5}$$

As the product $R(\mathrm{d}E/\mathrm{d}x)_{\mathrm{av}}$ is equal to the initial energy of α-particles, the α-annealing rate in the bulk can be expressed as

$$\mathrm{d}y = -c(T)y(E/2)\,\mathrm{d}D \tag{6}$$

and at the waste form surface as

$$dy = -c(T)y(E/4)\,dD. \quad (7)$$

When α-annealing is working, the disorder level in the bulk is governed by a balance between creation (Eq. (1)) and annealing rates (Eq. (6)):

$$dy/dD = V_0(T)[1-y] - yc(T)E/2. \quad (8)$$

As mentioned above, this equation cannot be used for a large amorphous fraction. When the disorder level increases, the creation rate which depends on the crystalline fraction decreases while the annealing rate increases. Therefore, an equilibrium can be reached at $dy = 0$ and the amorphous fraction at equilibrium, y_{eq}, is given by the following expression:

$$y_{eq} = V_0(T)/(V_0(T) + c(T)E/2). \quad (9)$$

Eq. (9) shows an interesting behavior of the α-annealing process characterized by the fact that the equilibrium disorder is independent on the concentration and half-life of the α-emitters since the α-flux and α-recoil number are always proportional in a given disordered volume.

2.3. Disorder thermal annealing in fluoroapatite

The plot of the defect recovery versus temperature in epitaxial recrystallization provides the thermal activation energies E_a and jump frequencies F. But in fluoroapatite, a direct measurement by RBS-C of thermal annealing of isolated disordered volumes cannot be achieved because of the high efficiency of the α-annealing process. Nevertheless by this technique, it has been possible to determine the thermal epitaxial regrowth kinetic of amorphous layers [23]. Determinations were performed in synthetic fluoroapatite single crystals along the c and $\langle 1\,1\,0\rangle$ axis by measuring the energy shift of the calcium rear edge for temperatures ranging between 350 and 560 °C. The different thermal annealing parameters E_a and F, are given in Table 1.

In case of isolated disordered volumes, it is necessary to transpose the thermal annealing kinetics that were obtained on amorphous layers to small isolated amorphous volumes present in the fluoroapatite matrix. From this extrapolation, it becomes possible to get the order of magnitude of the thermal annealing rate taking into account both, the total surface area of the isolated amorphous volumes and the thermal motion of the crystalline to amorphous interface.

Table 1
Jump frequencies (F) and activation energies (E_a) of thermal annealing of amorphous layers in fluoroapatite synthetic single crystals oriented along the c and $\langle 1\,1\,0\rangle$ axis

Orientation	E_a (eV)	F (cm/year)
c-axis	1.7	3.5×10^9
$\langle 1\,1\,0\rangle$	1.48	6.4×10^7

At equilibrium between creation and recovery, a cylindrical amorphous volume shape of 20 nm in length and of average volume $v = V_0(T)/2$ cm^3 with a surface area s cm^2 can be assumed. If y is the amorphous fraction, then the number of amorphous zones with an average volume v in a cubic centimeter is y/v, and their corresponding total surface area is $S = ys/v$ cm^2. Consequently, the annealed volume fraction is equal to $S\,dL$, where dL is the interface displacement which depends on the time increment dt and thermal annealing parameters of the amorphous layer (E_a,F). $S\,dL$ is expressed by

$$dy = -(s/v)yF\exp(-E_a/kT)\,dt. \quad (10)$$

This expression was chosen in agreement with our experimental results showing that the epitaxial regrowth of an amorphous layer versus time proceeds linearly. Nevertheless, this expression has not been clearly demonstrated to model the thermal recovery of the fission tracks [25]. Calculation with Eq. (10) gives only a crude evaluation of the thermal annealing rate in fluoroapatite because of uncertainties on the annealed interface area as well as on the recrystallization velocity at the interface, which has to be extrapolated from measurements performed at temperatures higher than 350 °C.

3. Fluoroapatite behavior modeling under repository conditions

The evolution of the relative damaged fraction in the actinide waste form can be expressed as a balance between defect creation and recovery rates. Combining Eqs. (1), (6) and (10) provides the variation, dy, of the amorphous fraction in a solid containing α-emitters as a function of the storage time:

$$dy = V_0(T)[1-y]\,dD - y[(s/v)F\exp(-E_a/kT)\,dt + c(T)(E/2)\,dD]. \quad (11)$$

As mentioned above, this equation is valid when amorphous volumes created by α-recoils can be taken as isolated. In a waste form loaded with 10 wt.% in concentration of actinide element, the number of atomic displacements (dpa) is approximately 20–30 times higher than the required amorphization dose in fluoroapatite and even higher if the daughter is a short-life nuclide. Then the waste form amorphization can occur at any time if the annealing processes are not efficient enough.

At the beginning of the disposal, a rather large temperature rise resulting from the high level of α-decay events may help to keep the waste form crystalline because of the reduction of the damage production and the increase of the annealing rate. But after one or two

half-life periods of time, the temperature will decrease and subsequently, the creation and annealing terms can change in a quite different way, whereas a large fraction of α-decays is still to come.

To get a disorder level evaluation during all the disposal time, it is necessary to take into account the temperature and radioactivity evolutions as a function of time. As for the moment, the repository temperature evolution is not yet well determined, the disorder evaluation will be established only for a constant temperature: 60 °C.

Under this condition, Eq. (11) can be rewritten as

$$\mathrm{d}y/\mathrm{d}t + y[\mathrm{d}D/\mathrm{d}t(V_0(T) + c(T)E/2) + R(T)] = V_0(T)\,\mathrm{d}D/\mathrm{d}t \tag{12}$$

with

$$R(T) = (s/v)F\exp(-E_a/kT),$$

where $\mathrm{d}D/\mathrm{d}t$ is the α-activity depending on the initial concentration N_0 and the half-life of the α-emitter as well as the half-life of its daughter. This differential equation can only be partially solved using the initial conditions: $y = 0$ and $D = 0$ at $t = 0$. Eq. (13) is obtained where the amorphous fraction, y, appears as a function of the cumulative dose D:

$$y = y_{eq}[1 - (1 + I(t)R(T))\exp(-V_0(T)D/y_{eq} - R(T)t)] \tag{13}$$

with

$$y_{eq} = V_0(T)/(V_0(T) + c(T)E_\alpha/2)$$

and

$$I(t) = \int_0^t \exp[(V_0(T)D/y_{eq} + R(T)u]\,\mathrm{d}u.$$

The integral $I(t)$ is undefined and a numeric calculation must be performed to determine y versus time.

Eq. (13) applies only in the case of a direct in-cascade amorphization and when the disordered volumes can be considered as isolated. When these conditions are fulfilled, the disorder at any time and temperature can be calculated and it becomes possible to adjust the disposal conditions in order to keep the disorder fraction at the safest level.

4. Numerical results in fluoroapatite and discussion

The equations established above can be used to calculate as a function of time the disorder level in a fluoroapatite matrix incorporating either ^{239}Pu ($t_{1/2} = 24,110$ years) or ^{244}Cm ($t_{1/2} = 18.1$ years).

In case of ^{239}Pu ($t_{1/2} = 24,110$ years) the daughter nuclei are ^{235}U ($t_{1/2} = 7 \times 10^8$ years) with a recoil energy of 88 keV. In view of its very long half-life, ^{235}U can be considered as stable and the cumulative dose, $D(t)$, versus time is given by

$$D(t) = N_0(1 - \exp(-\lambda_1 t)). \tag{14}$$

For ^{244}Cm, the daughter nuclei are ^{240}Pu atoms with a recoil energy of 95 keV. They decay with a lifetime of 6570 years to ^{236}U ($t_{1/2} = 2.4 \times 10^7$ years) which will be taken as stable. In this case $D(t)$ is expressed as

$$D(t) = \frac{N_0}{(\lambda_2 - \lambda_1)}[(\lambda_1 - 2\lambda_2)\exp(-\lambda_1 t) + \lambda_1\exp(-\lambda_2 t)] + 2N_0. \tag{15}$$

The α-annealing term is proportional to the α-particle energies that are equal to 5.15 MeV for ^{239}Pu and 5.8 and 5.16 MeV for ^{244}Cm and ^{240}Pu respectively. For this radioactive decay chain, since there is less than 2% mass difference between the two nuclei recoiling, the recoil energy and consequently $V_0(T)$ can be taken with a good approximation as proportional to the α-particle energy, E. If $V_0(T)$ and E vary in the same proportion, Eq. (9) shows that the α-particle energy variation has only a small influence on y_{eq}. Then, the α-particle energy and $V_0(T)$ values for the considered radionuclide can also be used for the daughter nucleus decay to make the calculation easier.

The disorder creation term depends on the amorphized volume created by each α-recoil (V_0). From TEM experiments [10], we have determined that the disordered volume produced by a 320 keV-Pb ion is equal to 3.3×10^{-19} cm^3 at 25 °C. As the energy density deposited along the track by 320 keV-Pb ions and α-recoil nuclei are comparable, the disordered volume can be assumed to be, at first approximation, proportional to the number of displaced atoms calculated by the SRIM-2000 code [26]. Then, the V_0 (25 °C) values for ^{244}Cm and ^{239}Pu are 1.14×10^{-19} cm^3 and 1.05×10^{-19} cm^3 respectively.

4.1. Effect of temperature on the defect creation and annealing rate

When the direct amorphization model applies, the V_0 variation versus temperature can be determined since $V_0(T)$ is inversely proportional to the critical amorphization doses which have been measured as a function of temperature for fluoroapatite [11,12]. If a disposal temperature of 60 °C is considered, the critical dose is increased by a factor of approximately 1.3 between 25 and 60 °C, and V_0 will be reduced by the same factor to give $V_0(60\ °C) = 8.8 \times 10^{-20}$ cm^3 for ^{244}Cm and $V_0(60\ °C) = 8.1 \times 10^{-20}$ cm^3 for ^{239}Pu.

From RBS experiments [9] in fluoroapatite, the volume recovery per eV at 25 °C is equal to $c(25\ °C) = 0.77 \times 10^{-25}$ cm^3/eV. Taking into account an α-anneal-

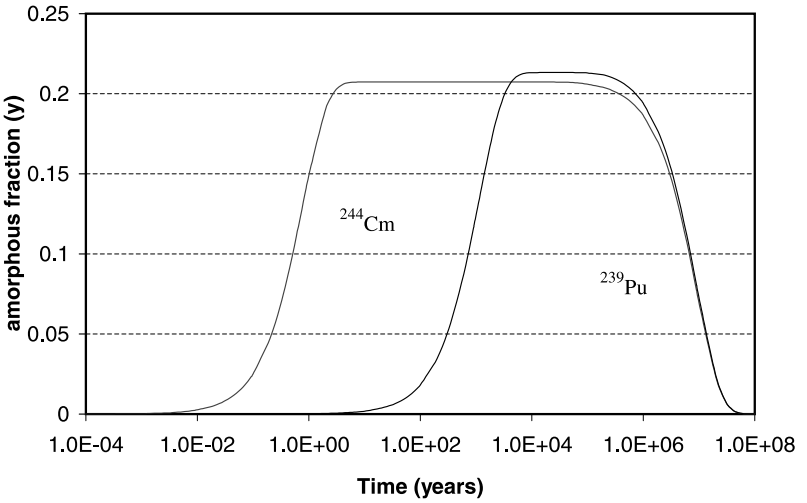

Fig. 2. Disorder level evolution as a function of time for fluoroapatite matrices loaded with 1 wt% of ^{244}Cm or ^{239}Pu at 60 °C.

ing thermal activation energy of approximately 0.1 eV [23], the annealing efficiency is increased by a factor 1.5 at 60 °C and $c(60\ ^\circ\text{C}) = 1.16 \times 10^{-25}$ cm^3/eV.

The thermal annealing rate at 60 °C is obtained by extrapolation of annealing kinetics data measured at high temperature on an amorphous layer [23] (Table 1). For $\langle 1\,1\,0\rangle$ and c-axis orientation, it is estimated to be 2.7×10^{-15} cm/year and 7×10^{-17} cm/year, respectively. For isolated defects, all crystalline orientations are present but the fastest process occurring in this case along the $\langle 1\,1\,0\rangle$ direction will direct the annealing kinetics. Then, with an amorphous average volume $v = V_0(60\ ^\circ\text{C})/2 \approx 4 \times 10^{-20}$ cm^3 which corresponds to a surface $s \approx 10^{-12}$ cm^2, the value $R(60\ ^\circ\text{C}) = 7 \times 10^{-8}$ cm^{-1}/year can be used in Eq. (13). This disorder thermal recovery rate corresponds to a defect lifetime of 10 million years. This value obtained by extrapolation of measurements performed at much higher temperatures, is affected by large uncertainties. But, the long defect lifetime shows that thermal annealing in fluoroapatite is negligible compared to α-annealing except for very low α-decay rate. If the defect lifetime is long enough, the disorder level will remain constant for a long time, even if the α-decay rate is close to zero.

4.2. Disorder evaluation in fluoroapatite containing ^{244}Cm or ^{239}Pu

With the above experimentally determined parameters at 60 °C, Eq. (13) which gives the disorder level evolution as a function of time, can be used for fluoroapatite matrices loaded with 1% in weight of ^{244}Cm or ^{239}Pu (Fig. 2). When actinides are introduced in fluoroapatite at this level, a chemical composition modification is necessary to maintain the charge balance. But for this preliminary approach of the disorder evolution, one assumes that this chemical modification does not change the creation and annealing rates.

Fig. 2 shows that for both actinides, the disorder reaches a plateau which level depends weakly on α-energies. This disorder level corresponds to an amorphous fraction close to 20% and is independent of the dose rate. The time delay in reaching the equilibrium regime is proportional to the lifetime of the nuclide of interest and inversely proportional to its concentration. The delay corresponds approximately to a dose of 10^{19} α-decay events per cubic centimeter. At the end of the α-emitter life, the dose rate becomes negligible and the thermal annealing becomes predominant. As a consequence, the disorder decreases slowly until it goes close to zero.

Comparisons with already published data [5] are quite difficult because of (i) different compositions of investigated apatite hosts: i.e. fully phosphate fluoroapatite and fully silicate oxoapatite, (ii) the α-annealing effect operates in phosphate fluoroapatite but not in silicate oxoapatite since this matrix loaded with ^{244}Cm readily get amorphous [27,28], excluding an efficient α-annealing effect.

5. Conclusion

The crystalline state in natural phosphate apatites having experienced high α-decay doses, is due to α-annealing and thermal annealing acting simultaneously with efficiencies depending on temperature and dose rate conditions. Following the data listed in Table 1 for temperatures close to ambient, α-annealing can be considered as the dominant process of recovery since the thermal disorder lifetime is evaluated to 10^7–10^8 years. On the contrary, at higher temperature (>60 °C), the

thermal annealing has an activation energy 15 times larger than α-annealing (≈1.5 eV instead of ≈0.1 eV) and therefore both annealing effects will cooperate to avoid amorphization.

For actinide immobilization, the situation is different since the α-decay doses and dose rates will be much higher than in minerals. But, as it is shown through the present study, due to a dominant α-annealing process, the total amorphization of fluoroapatite loaded with α-emitters will never occur over geologic periods whatever the actinide content may be. Actually, at a given temperature, the disorder induced by α-recoils reaches an equilibrium level independent of the dose rate. Therefore, the actinide content is not a critical parameter in fluoroapatite as far as the amorphization is concerned. Nevertheless more accurate data on the disorder creation and annealing efficiency are still needed. For example, the thermal annealing should be measured at temperatures lower than 350 °C in order to improve the data extrapolation at disposal temperature. In the same way, the disorder creation term should be measured as a function of temperature.

To introduce significant amount (10 wt%) of actinides in ($Ca_{10}(PO_4)_6F_2$), it is necessary to modify the chemical composition of the host. For example, silicate groupings can be introduced in the structure using the substitution of (PO_4^{3-}, Ca^{2+}) by (SiO_4^{4-}, RE^{3+} or/and An^{3+}). The following apatite composition [3,7,29]: $Ca_9RE_{1-x}An_x(PO_4)_5(SiO_4)F_2$ can be considered as an actinide host phase. This compound is a mono-silicated fluoroapatite and our studies are now focused on this apatite composition [7,30].

Acknowledgements

We gratefully acknowledge the assistance of the technical staff of the ARAMIS accelerator and the IRMA implanter, as well as Professor H. Bernas for useful discussions. This work is a part of the PhD studies of S.S. who is supported by the French Commissariat à l'Energie Atomique.

References

[1] J. Carpena, J.L. Lacout, French patent 93 08676, 1993.
[2] R.C. Ewing, W.J. Weber, W. Lutze, in: E.R. Merz, C.E. Walter (Eds.), Disposal of Weapons Plutonium, Kluwer Academic, Netherlands, 1996, p. 65.
[3] J. Carpena, L. Boyer, J.L. Lacout, French Patent 98 11334, 1998.
[4] W.J. Weber, J. Am. Ceram. Soc. 65 (11) (1982) 544.
[5] W.J. Weber, R.C. Ewing, A. Meldrum, J. Nucl. Mater. 250 (1997) 147.
[6] J. Carpena, J.R. Kienast, K. Ouzegane, C. Jehanno, Geol. Soc. Am. Bull. 100 (1998) 1237.
[7] S. Soulet, J. Carpena, J. Chaumont, J.C. Krupa, M.O. Ruault, J. Nucl. Mater. 299 (2001) 227.
[8] K. Trachenko, M.T. Dove, E. Salje, J. Appl. Phys. 87 (2000) 7702.
[9] S. Ouchani, J.-C. Dran, J. Chaumont, Nucl. Instrum. and Meth. Phys. Res B 132 (1997) 447.
[10] S. Soulet, J. Chaumont, J.C. Krupa, J. Carpena, M.O. Ruault, J. Nucl. Mater. 289 (2001) 194.
[11] R.C. Ewing, L.M. Wang, W.J. Weber, Mater. Res. Soc. Proc. 373 (1995) 347.
[12] L.M. Wang, M. Cameron, W.J. Weber, K.D. Crowley, R.C. Ewing, in: P.W. Brown, B. Constantz (Eds.), Hydroxyapatite and Related Materials, CRC, New York, 1994, p. 243.
[13] L.M. Wang, W.J. Weber, Philos. Mag. A 79 (1) (1999) 237.
[14] G. Carter, R. Webb, Radiat. Eff. Lett. 43 (1979) 19.
[15] W.J. Weber, J. Mater. Res. 5 (11) (1990) 2687.
[16] A. Meldrum, L.A. Boatner, R.C. Ewing, Phys. Rev. 56 (21) (1997) 13805.
[17] S.X. Wang, L.M. Wang, R.C. Ewing, G.S. Was, G.R. Lumpkin, Nucl. Instrum. and Meth. Phys. Res. B 148 (1999) 704.
[18] A. Meldrum, S.J. Zinkle, L.A. Boatner, R.C. Ewing, Nature 395 (1998) 56.
[19] A. Meldrum, L.A. Boatner, S.J. Zinkle, S.X. Wang, L.M. Wang, R.C. Ewing, Can. Mineral. 37 (1999) 207.
[20] W.J. Weber, L.M. Wang, N. Yu, Nucl. Instrum. and Meth. Phys. Res. B (1996).
[21] W.J. Weber, L.M. Wang, Nucl. Instrum. and Meth. Phys. Res B 106 (1995) 298.
[22] A. Meldrum, L.A. Boatner, R.C. Ewing, Nucl. Instrum. and Meth. Phys. Res. B 141 (1998) 347.
[23] S. Ouchani, PhD thesis, University Paris XI, 1997.
[24] A. Meldrum, L.A. Boatner, R.C. Ewing, Mater. Res. Soc. Symp. Proc. 439 (1996).
[25] P.F. Green, I.R. Duddy, G.M. Laslett, Earth Planet. Sci. Lett. 87 (1988) 216.
[26] J.F. Ziegler, J.P. Biersack, D.J. Marwick, SRIM: The Stopping and Range of Ions in Matters, IBM Corporation, New York, 2000.
[27] W.J. Weber, J. Am. Ceram. Soc. 76 (1993) 1729.
[28] W.J. Weber, Nucl. Instrum. and Meth. Phys. Res. B 65 (1992) 88.
[29] C. Meis, J.D. Gale, L. Boyer, J. Carpena, D. Gosset, J. Phys. Chem. B 104 (2000) 5380.
[30] S. Soulet, J. Carpena, J. Chaumont, O. Kaitasov, J.C. Krupa, M.O. Ruault, Nucl. Instrum. and Meth. Phys. Res. B 184 (3) (2001) 383.